JACS
JOURNAL OF THE AMERICAN CHEMICAL SOCIETY
Communication
pubs.acs.org/JACS

Alkaline Phosphatase-Triggered Simultaneous Hydrogelation and Chemiluminescence

Zijuan Hai, Jindan Li, Jingjing Wu, Jiacheng Xu, and Gaolin Liang*

CAS Key Laboratory of Soft Matter Chemistry, Department of Chemistry, University of Science and Technology of China, 96 Jinzhai Road, Hefei, Anhui 230026, China

Supporting Information

ABSTRACT: Chemiluminescence (CL) has a higher signal-to-noise ratio than fluorescence, but the use of CL to track an enzyme-instructed self-assembly (EISA) process has not been reported. In this work, by coincubation of the hydrogelator precursor Fmoc-Phe-Phe-Tyr(H_2PO_3)-OH (**1P**) and the CL agent AMPPD (**2**) with alkaline phosphatase (ALP), we employed CL to directly characterize and image the simultaneous EISA process of **1P**. Hydrogelation processes of **1P** with and without **2** and the CL properties of **2** with and without **1P** under ALP catalysis were systematically studied. The results indicated that **2** is an ideal CL indicator for ALP-triggered hydrogelation of **1P**. Using an IVIS optical imaging system, we obtained time-course CL images of **2** to track the simultaneous hydrogelation process of **1P** in the same solution. We envision that our CL method could be employed to track more biological EISA events in the near future.

Supramolecular hydrogels, one type of biomaterials formed by the self-assembly of small molecules to gel large amount of water (more than 95 wt %),[1−3] have been extensively explored in recent decades and have found wide biomedical applications in drug delivery,[4,5] tissue engineering,[6] wound healing,[7] cell fate control,[8] metal ion absorption,[9] biomarker sensing,[10−13] functional materials design,[14] etc. The methods to fabricate hydrogels are roughly categorized into physical hydrogelation (e.g., pH, temperature, ionic strength), chemical initiation (e.g., ligand−receptor interactions, in situ formation of hydrogelators), and enzymatic regulation. Among them, enzyme-instructed self-assembly (EISA) of hydrogels has drawn increased attention because of its inherent biocompatibility and bionics.[15] When a hydrogelator is tagged by a fluorophore, its enzymatic hydrogelation process accompanied by a fluorescence turn "on" or "off" can in turn be employed to monitor the enzyme activity[16,17] or an intracellular process.[18,19]

As we know, however, when applied for biomedical applications, fluorescence suffers from photobleaching of the fluorophores, background interference, and autofluorescence from the detected samples. Thus, an EISA process might not be precisely demonstrated by a fluorescent hydrogelator. In contrast to fluorescence, chemiluminescence (CL) does not require light excitation, and thus, its signal-to-noise ratio is greatly improved because of the reduction or suppression of autofluorescence.[20] However, to the best of our knowledge there has been no report of the use of CL to characterize (or image) a hydrogelation process.

Alkaline phosphatase (ALP) is an important, highly efficient enzyme that is responsible for cleavage of the phosphate groups from its substrate molecules. It has been widely used for EISA of nanofibers extracellularly and intracellularly.[18,21] Interestingly, ALP is also the enzyme that dephosphorylates 3-(2′-spiroadamantyl)-4-methoxy-4-(3″-phosphoryloxyphenyl)-1,2-dioxetane (AMPPD, **2**) to yield adamantan-2-one (**3**) and the electronically excited fluorophore *m*-oxybenzoate ion (**4**), which emits a CL photon at 470 nm (Figure 1).[22] Thus, in this work, we incubated an efficient hydrogelator precursor, Fmoc-Phe-Phe-Tyr(H_2PO_3)-OH (**1P**),[23] and **2** with ALP and found that the CL from **2** could well be applied to characterize the simultaneous ALP-instructed hydrogelation of **1P** (Figure 1).

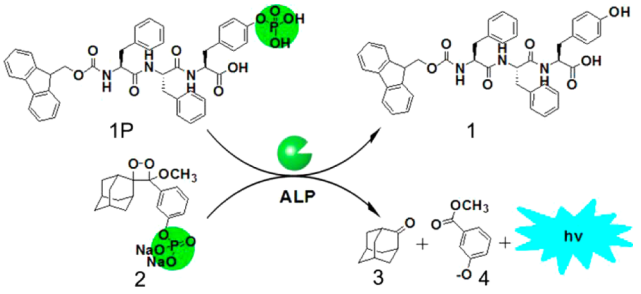

Figure 1. Schematic illustration of ALP-triggered simultaneous hydrogelation of **1P** and chemiluminescence of **2**.

We began the study with the syntheses of the precursor **1P** and the hydrogelator Fmoc-Phe-Phe-Tyr-OH (**1**) (Schemes S1 and S2). They were directly synthesized by solid-phase peptide synthesis (SPPS) and purified by high-performance liquid chromatography (HPLC) (Figures S1−S6). After the syntheses, we first obtained the kinetic parameters of **1P** and **2** for their ALP-catalyzed dephosphorylation reactions, respectively. Using Fmoc-Gly-OH and Fmoc-Val-OH as internal standards, we obtained the HPLC peak area calibration curves for **1P** and **2** at 254 and 280 nm, respectively (Figures S7 and S8). Excess **1P** or **2** at different concentrations was incubated with 3×10^{-9} M ALP at 25 °C for 3 min in ALP buffer (50 mM Tris-HCl, 1 mM $MgCl_2$, pH 9.6). Then the initial velocities were plotted against the initial concentrations of **1P** or **2** and fitted to the

Received: October 22, 2016
Published: January 8, 2017

DOI: 10.1021/jacs.6b11041
J. Am. Chem. Soc. 2017, 139, 1041−1044

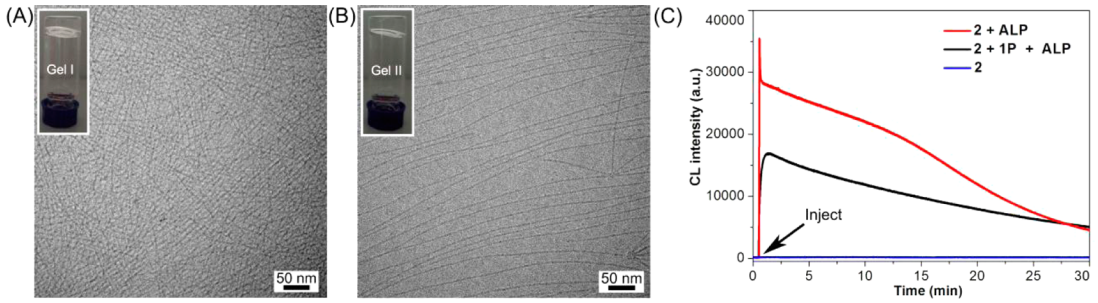

Figure 2. (A) Cryo-TEM image of gel **I** (inset: photograph of gel **I**). (B) Cryo-TEM image of gel **II** (inset: photograph of gel **II**). (C) CL kinetic curves of 1.25 mM **2** (blue), 1.25 mM **2** with 2 μM ALP (red), and 1.25 mM **2** and 12.9 mM **1P** with 2 μM ALP (black) at 25 °C in ALP buffer with static injection.

Michaelis–Menten model (Figures S9 and S10). Using Lineweaver–Burk analysis, we obtained the k_{cat}/K_M values for **1P** (2.01×10^6 M^{-1} s^{-1}) and **2** (1.80×10^6 M^{-1} s^{-1}), which are close to each other (Table S1), suggesting that **1P** and **2** are subjected to a comparable speed of dephosphorylation by ALP. Thus, we concluded that **2** should be an ideal CL indicator for tracking the ALP-triggered EISA process of **1P**.

ALP-triggered hydrogelation of **1P** was then tested. In brief, 1 wt % **1P** (12.9 mM) and 26.0 mM Na_2CO_3 were dissolved in 300 μL of ALP buffer as a clear solution. After incubation with 2 μM ALP for 15 min at 25 °C, the solution changed to a transparent hydrogel, gel **I** (inset of Figure 2A). The inverted-tube test indicated that the critical gelation concentration (CGC) for gel **I** was 6.5 ± 0.5 mM (Figure S11A). A plot of transmittance at 600 nm versus the concentration of gel **I** revealed two regimes, indicating that its critical micelle concentration (CMC) was 33 μM (Figure S11B). HPLC analysis indicated that 78.0% of the precursor **1P** was converted to hydrogelator **1** by 2 μM ALP after 30 min of incubation (Figure S12).

Then the gelation ability of the mixture of **1P** and **2** was tested. **1P** (1 wt %, 12.9 mM), 1.25 mM **2**, and 26.0 mM Na_2CO_3 were dissolved in 300 μL of ALP buffer as a clear solution, sol **II** (Figure S13A). After incubation with 2 μM ALP at 25 °C, the clear solution turned to a turbid solution at 1 min (Figure S13B), a turbid hydrogel at 15 min (Figure S13C), and finally a transparent gel, gel **II**, at 30 min (inset of Figure 2B). This clear–turbid–transparent process was also observed by direct incubation of the clear solution of **2** with ALP, which turned to a turbid solution from 1 to 15 min but returned to a clear solution at 30 min (Figure S13D–F). The CGC and CMC for gel **II** were measured to be 5.5 ± 0.5 mM and 24 μM (Figure S11C,D), both of which are lower than those of gel **I**, suggesting that **1P** is more prone to self-assembly in sol **II** than in **1P** solution.

To study the enzymatic processes of gel **I** and gel **II**, dynamic time sweeps were chosen to examine the changes in viscoelasticity of the **1P** solution and sol **II**, respectively. As shown in Figure S14, after incubation with 2 μM ALP, both the storage modulus (G') and the loss modulus (G'') of the solutions gradually increased with time, and the G' values started to dominate over the G'' values at around 39 s for the **1P** solution (Figure S14A) and around 91 s for sol **II** (i.e., **1P** and **2**) (Figure S14B), suggesting the approaches to their gelling points. Because of the competitive ALP consumption by **2**, the hydrogelation process of sol **II** was delayed compared with that of the **1P** solution. Interestingly, both the G' and G'' values for gel **II** were 1 order of magnitude higher than those for gel **I**, suggesting that the enzymatic products of **2** (i.e., **3** and **4**) did not interfere with but rather enhanced the self-assembly of **1** to form gel **II**.

After rheology tests, we performed cryo transmission electron microscopy (cryo-TEM) to study the internal networks in the hydrogels. Gel **I** exhibited short, thin, entangled nanofibers with an average width of 3.8 ± 0.5 nm (Figures 2A and S15A). Gel **II** showed long, wide, regular nanofibers with an average width of 4.3 ± 0.5 nm (Figures 2B and S15B). The difference between the fiber widths of gels **I** and **II** might be caused by the interference of **4** with the molecular arrangement of hydrogelator **1**. In our previous model,[23] molecules of **1** centripetally stack to form the hydrophobic inner tubular layer, and its peptide segments stretch into the surrounding water to form the hydrophilic outer layer of the nanofiber. However, in gel **II**, molecules of **4** might π–π stack with the tyrosine motifs of **1** because of their structural similarity, resulting in the extension of the hydrophilic layer of the nanofiber.[24] Circular dichroism (CD) spectroscopy measurements indicated that gel **I** exhibited a similar spectrum as gel **II** (Figure S16). A negative Cotton effect at 214 nm indicated the formation of β-sheet-like secondary structure in the nanofibers. Two troughs at 242 and 275 nm suggested the chiral arrangement of the aromatic side chains of the hydrogelator.[21]

The CL properties of **2** in solution and sol **II** (i.e., **1P** and **2**) were investigated after static injections of ALP. CL kinetic curves of **2** with and without different concentrations of ALP at 25 °C were studied first. As shown in Figure S17A, in the absence of ALP, a CL signal of **2** in solution was not observed. When different concentrations of ALP were injected, obvious CL emissions were observed. Briefly, with increasing ALP concentration (from 2 to 200 nM) injected, the solution of **2** reached its CL peaks faster, and they were higher (Figure S17A). At a fixed ALP concentration of 2 μM, CL kinetic curves of **2** at different concentrations (from 0.5 to 1.5 mM) reached their peaks at the same time of 5 s, but their intensities increased with increasing concentration of **2** (Figure S17B), suggesting that 2 μM ALP is largely excessive. HPLC together with electrospray ionization/mass analyses indicated that 1.25 mM **2** was completely converted to compounds **3** and **4** by 2 μM ALP after 30 min of incubation (Figures S18–S20). At an ALP concentration of 2 μM, while the CL kinetic curve of **2** reached its peak value (35509) at 5 s, the CL curve of sol **II** reached its peak value (16201) at 60 s (Figure 2C). The delayed and decreased CL intensity of **2** in sol **II** should be ascribed to the competitive ALP consumption by **1P** in the solution. With a decrease in the ALP concentration, both the gelling time (221 s for 1 μM ALP and 598 s for 0.4 μM ALP)

DOI: 10.1021/jacs.6b11041
J. Am. Chem. Soc. 2017, 139, 1041–1044

and the CL peak time (114 s for 1 μM ALP and 260 s for 0.4 μM ALP) of sol **II** were significantly delayed (Figures S21 and S22).

As we mentioned above, at 2 μM ALP, **2** delayed the enzymatic gelling point of **1P** from 39 to 91 s (52 s interval) while **1P** delayed the CL peak of **2** from 5 to 60 s (55 s interval). Thus, during a long time observation, we assume that the CL signal of **2** could well be employed to directly visualize the simultaneous ALP-triggered hydrogelation process of **1P**. Sol **II** in an Eppendorf tube was placed in an IVIS optical imaging system. Upon the addition of 2 μM ALP to the solution, time-course CL images of the tube were taken. As shown in Figure 3, at 1 min, a large area of CL signal, with a

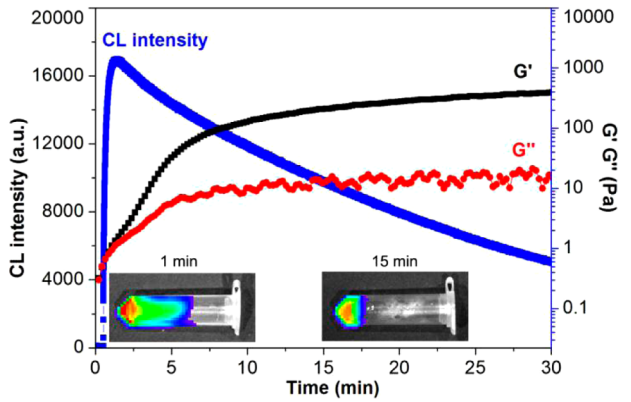

Figure 3. CL kinetic curve and dynamic time sweep of 12.9 mM **1P** and 1.25 mM **2** incubated with 2 μM ALP at 25 °C in ALP buffer. Insets: time-course CL images of sol **II** (i.e., **1P** and **2**) incubated with ALP at 25 °C in ALP buffer.

calculated total of 2.2×10^5 photons, was observed in the tube (left inset of Figure 3), which suggests the sample remained in the liquid state. At 15 min, the CL signal of the sample was concentrated at the bottom of the tube, with a calculated total of 9.8×10^4 photons (right inset), which suggests the formation of gel **II**. The transition of sol **II** to gel **II** could be directly photographed by the machine (data not shown).

To find an exact substrate ratio at which the CL peak can be employed for the precise monitoring of the hydrogelation process, at a fixed **1P** concentration of 12.9 mM and ALP concentration of 2 μM we changed the amount of **2** from 0.5 to 0.75, 1.0, 1.25, and 1.5 mM, obtaining five solutions with different **2**/**1P** ratios ranging from 0.039 to 0.116, and characterized their hydrogelation and CL processes. The results indicated that the higher the concentration of **2** was, the solution reached its gelling point slower (from 53 to 109 s; Figure S23) but its CL peak faster (from 90 to 45 s; Figure S24). Plots of the times required to reach the gelling point or CL peak against the **2**/**1P** ratio showed two lines with an intersection of 75 s at a **2**/**1P** ratio of 0.071 (Figure S25). This suggests that at a **2**/**1P** ratio of 0.071 the CL peak of **2** could be employed to precisely characterize the hydrogelation process of **1P**.

Moreover, we also could quantitatively correlate the CL signal with the hydrogelation process. For example, at 20 min, the above five solutions with different **2**/**1P** ratios were injected into an HPLC to calculate the conversion percentages of **1P** (Figure S26). Correlation of the **1P** conversion with the **2**/**1P** ratio showed a negative linear relationship ($Y = 58.22 - 81.14X$, $R^2 = 0.956$; Figure S27A). When we calculated the total CL photons for these five mixtures in 20 min (Figure S24) and correlated their photon percentages with the **2**/**1P** ratio (using the largest photon number as 100%), a positive linear relationship was obtained ($Y = -3.61 + 886.04X$, $R^2 = 0.996$; Figure S27B). Thus, the equation (CL photon percentage) + 10.92 × (conversion percentage of **1P**) = 632.15 was obtained for quantitative correlation of the CL signal with the hydrogelation process at 20 min.

In summary, by coincubation of hydrogelator precursor **1P** and CL agent **2** with ALP, we employed CL to directly characterize and image the simultaneous hydrogelation process. The k_{cat}/K_M values of the ALP-catalyzed dephosphorylation reactions of **1P** and **2** are close to each other, suggesting that **2** should be an ideal CL indicator for ALP-triggered hydrogelation of **1P**. By altering the amount of **2**, we found that at a **2**/**1P** ratio of 0.071 sol **II** reached its CL peak and gelling point simultaneously. Using an IVIS optical imaging system, we obtained time-course CL images of **2** to track the simultaneous hydrogelation process of **1P** in the same solution. Interestingly, even when an anticancer drug (e.g., doxorubicin) was added into the system, we still could use the CL to track the hydrogelation process (Figure S28). We envision that the CL method described herein could be employed to track more biological EISA events in the near future.

■ ASSOCIATED CONTENT

Supporting Information

The Supporting Information is available free of charge on the ACS Publications website at DOI: 10.1021/jacs.6b11041.

General methods, syntheses and characterizations of **1P** and **1**, Figures S1−S28, and Tables S1−S3 (PDF)

■ AUTHOR INFORMATION

Corresponding Author

*gliang@ustc.edu.cn

ORCID

Gaolin Liang: 0000-0002-6159-9999

Notes

The authors declare no competing financial interest.

■ ACKNOWLEDGMENTS

This work was supported by the Collaborative Innovation Center of Suzhou Nano Science and Technology, Hefei Science Center CAS (2016HSC-IU010), the Ministry of Science and Technology of China (2016YFA0400904), and the National Natural Science Foundation of China (Grants 21675145 and U1532144).

■ REFERENCES

(1) Berger, O.; Adler-Abramovich, L.; Levy-Sakin, M.; Grunwald, A.; Liebes-Peer, Y.; Bachar, M.; Buzhansky, L.; Mossou, E.; Forsyth, V. T.; Schwartz, T.; Ebenstein, Y.; Frolow, F.; Shimon, L. J. W.; Patolsky, F.; Gazit, E. *Nat. Nanotechnol.* **2015**, *10*, 353.

(2) Zhang, Y.; Zhou, N.; Shi, J.; Pochapsky, S. S.; Pochapsky, T. C.; Zhang, B.; Zhang, X.; Xu, B. *Nat. Commun.* **2015**, *6*, 6165.

(3) Versluis, F.; van Esch, J. H.; Eelkema, R. *Adv. Mater.* **2016**, *28*, 4576.

(4) Liang, G. L.; Yang, Z. M.; Zhang, R. J.; Li, L. H.; Fan, Y. J.; Kuang, Y.; Gao, Y.; Wang, T.; Lu, W. W.; Xu, B. *Langmuir* **2009**, *25*, 8419.

(5) Tian, Y.; Wang, H. M.; Liu, Y.; Mao, L. N.; Chen, W. W.; Zhu, Z. N.; Liu, W. W.; Zheng, W. F.; Zhao, Y. Y.; Kong, D. L.; Yang, Z. M.; Zhang, W.; Shao, Y. M.; Jiang, X. Y. *Nano Lett.* **2014**, *14*, 1439.

DOI: 10.1021/jacs.6b11041
J. Am. Chem. Soc. 2017, 139, 1041−1044

(6) Ren, K. X.; He, C. L.; Xiao, C. S.; Li, G.; Chen, X. S. *Biomaterials* **2015**, *51*, 238.
(7) Ghobril, C.; Charoen, K.; Rodriguez, E. K.; Nazarian, A.; Grinstaff, M. W. *Angew. Chem., Int. Ed.* **2013**, *52*, 14070.
(8) Wang, H.; Feng, Z.; Wu, D.; Fritzsching, K. J.; Rigney, M.; Zhou, J.; Jiang, Y.; Schmidt-Rohr, K.; Xu, B. *J. Am. Chem. Soc.* **2016**, *138*, 10758.
(9) Miao, Q. Q.; Wu, Z. Y.; Hai, Z. J.; Tao, C. L.; Yuan, Q. P.; Gong, Y. D.; Guan, Y. F.; Jiang, J.; Liang, G. L. *Nanoscale* **2015**, *7*, 2797.
(10) Cai, Y. B.; Shi, Y.; Wang, H. M.; Wang, J. Y.; Ding, D.; Wang, L.; Yang, Z. M. *Anal. Chem.* **2014**, *86*, 2193.
(11) Zhai, D. Y.; Liu, B. R.; Shi, Y.; Pan, L. J.; Wang, Y. Q.; Li, W. B.; Zhang, R.; Yu, G. H. *ACS Nano* **2013**, *7*, 3540.
(12) Wang, H. M.; Wang, Y. Z.; Zhang, X. L.; Hu, Y. W.; Yi, X. Y.; Ma, L. S.; Zhou, H.; Long, J. F.; Liu, Q.; Yang, Z. M. *Chem. Commun.* **2015**, *51*, 14239.
(13) Cai, Y. B.; Zhan, J.; Shen, H. S.; Mao, D.; Ji, S. L.; Liu, R. H.; Yang, B.; Kong, D. L.; Wang, L.; Yang, Z. M. *Anal. Chem.* **2016**, *88*, 740.
(14) Lee, J.; Peng, S. M.; Yang, D. Y.; Roh, Y. H.; Funabashi, H.; Park, N.; Rice, E. J.; Chen, L. W.; Long, R.; Wu, M. M.; Luo, D. *Nat. Nanotechnol.* **2012**, *7*, 816.
(15) Yang, Z.; Liang, G.; Xu, B. *Acc. Chem. Res.* **2008**, *41*, 315.
(16) Han, A. T.; Wang, H. M.; Kwok, R. T. K.; Ji, S. L.; Li, J.; Kong, D. L.; Tang, B. Z.; Liu, B.; Yang, Z. M.; Ding, D. *Anal. Chem.* **2016**, *88*, 3872.
(17) Ren, C. H.; Wang, H. M.; Mao, D.; Zhang, X. L.; Fengzhao, Q. Q.; Shi, Y.; Ding, D.; Kong, D. L.; Wang, L.; Yang, Z. M. *Angew. Chem., Int. Ed.* **2015**, *54*, 4823.
(18) Gao, Y.; Shi, J. F.; Yuan, D.; Xu, B. *Nat. Commun.* **2012**, *3*, 1033.
(19) Zhou, J.; Du, X. W.; Li, J.; Yamagata, N.; Xu, B. *J. Am. Chem. Soc.* **2015**, *137*, 10040.
(20) Richard, J. A.; Jean, L.; Schenkels, C.; Massonneau, M.; Romieu, A.; Renard, P. Y. *Org. Biomol. Chem.* **2009**, *7*, 2941.
(21) Zheng, Z.; Chen, P.; Xie, M.; Wu, C.; Luo, Y.; Wang, W.; Jiang, J.; Liang, G. *J. Am. Chem. Soc.* **2016**, *138*, 11128.
(22) Tu, L. P.; Wang, Y.; Yang, Y. F.; Bakker, B. H.; Kong, X. G.; Brouwer, A. M.; Buma, W. J.; Zhang, H. *Phys. Chem. Chem. Phys.* **2010**, *12*, 6789.
(23) Wang, W. J.; Qian, J. C.; Tang, A. M.; An, L. N.; Zhong, K.; Liang, G. L. *Anal. Chem.* **2014**, *86*, 5955.
(24) Yu, Z. L.; Tantakitti, F.; Yu, T.; Palmer, L. C.; Schatz, G. C.; Stupp, S. I. *Science* **2016**, *351*, 497.

DOI: 10.1021/jacs.6b11041
J. Am. Chem. Soc. 2017, 139, 1041−1044